IEEE Access
Multidisciplinary | Rapid Review | Open Access Journal

Received September 15, 2020, accepted September 25, 2020, date of publication October 6, 2020, date of current version October 15, 2020.

Digital Object Identifier 10.1109/ACCESS.2020.3029050

Radiation Enhancement of an Ultrawideband Unidirectional Folded Bowtie Antenna for GPR Applications

GUANGYAO YANG[1,2], (Student Member, IEEE), SHENGBO YE[1], YICAI JI[1,2], XIAOJUAN ZHANG[1], AND GUANGYOU FANG[1,2]

[1]Key Laboratory of Electromagnetic Radiation and Sensing Technology, Aerospace Information Research Institute, Chinese Academy of Sciences, Beijing 100190, China
[2]School of Electronic, Electrical and Communication Engineering, University of the Chinese Academy of Sciences, Beijing 100039, China

Corresponding author: Shengbo Ye (shengboye@163.com)

This work was supported in part by the ZFS under Grant Y9E0151M26.

ABSTRACT An arc-shaped distributed multilayer capacitive loading structure combined with resistive loading is presented in this paper to enhance the radiation performance of folded bowtie antenna (FBA). The radiation efficiency of the loaded bowtie antenna (BA) is improved, and the low-frequency bandwidth is broadened by the bent loop circuits. Additionally, a novel technique of cavity groove is proposed to design the reflector. The optimized cavity tightly coupling with the radiation part overcomes the shortcomings of conventional cavity-backed BAs. The improved ultra-wideband (UWB) FBA with low profile is then designed and fabricated. The basic geometry of the proposed antenna is combined by a novel acorn-shaped bent bowtie patch and a hollowed stepped back cavity. The simulated -10 dB impedance bandwidth of the proposed antenna is over 100 MHz-1100 MHz while the measured operating bandwidth is 250 MHz-850 MHz. This BA of folded type obtains a high realized gain of 4 dBi at 850 MHz and a narrow pattern over the whole band. Time-domain measurements and field tests for practical ground-penetrating radar (GPR) applications have been carried out and the results demonstrate the advanced performance.

INDEX TERMS Ultra-wideband (UWB), ground-penetrating radar (GPR), P-band, miniaturized antenna, folded bowtie antenna, RC-loading, radiation enhancement.

I. INTRODUCTION

Ground-penetrating radar (GPR) is a well-accepted geophysical technique. Initially applied to detect natural geologic materials, now GPR is equally well applied to a host of other media such as wood, concrete, and asphalt. The existence of numerous lossy dielectric material environments, combined with the broad radio frequency spectrum, leads to a wide range of nondestructive testing (NDT) applications, such as archaeology, geophysical research, road quality assessment, buried objects detection, and civil engineering. [1]

GPR systems can be categorized into two types, first are ones that transmit continuous wave and work in frequency domain. The second type is impulse wave GPR systems that work in time domain. Impulse-based radar systems are cost-effective and have simple design, therefore this type of system is preferred in commercial GPR applications. [2] The antenna system is one of the most critical parts of the GPR system. Ultra-wideband technology, which was used in the field of wireless communication early on, has now been applied to the field of GPR by many researchers because of the strong penetrability and better resolution. In the FCC Part 15 rules, the demarcation between wideband and UWB was decreased to 0.20 (20%), while the OSD/DARPA Review Panel states that signals having fractional bandwidths greater than 0.25 (25%) are UWB signals. Typical UWB antennas applied for impulse GPR cover broad bandwidth from megahertz to gigahertz. In pursuit of extremely high distance resolution, UWB GPRs commonly use a frequency range above 100MHz with a 100% fractional bandwidth. [3] The low operating frequency radiation is necessary, especially for applications that need to detect through invisible lossy medium [1]. The radiation at higher frequency above 1GHz can give a higher resolution, whereas cannot propagate far and the depth of detection becomes shallower. However, according to the principle of antennas, low cut-off frequency, in the sense of

The associate editor coordinating the review of this manuscript and approving it for publication was Francesco Benedetto.

antenna matching, corresponds to a large size. [4] In many scenarios, The GPR antennas are limited by their huge profile. Thus, miniaturization of the UWB antenna remains an interesting topic in research. In this field, antenna size, matching, and radiation efficiency conflict with each other. Gain is a widely used antenna parameter combined with directivity and efficiency. It is a far-field characterization of antenna radiation. But for the GPR antenna, the true performance cannot be revealed properly by gain and gain pattern when the lossy materials are involved. The targets to be detected are usually buried in the near-field area of the antenna. And the proximity of the antenna to the ground means that it is necessary to consider the coefficients of reflection and transmission as the wave passes through the dielectric to the target. [1] There is a near-field feature called footprint that can represent the energy coupling into the dielectric in a graphical manner. An antenna footprint is defined as a distribution of the normalized peak values of transmit waveforms within a horizontal plane on the ground surface or subsurface, which indicates the shape and size of the spot illuminated by the antenna. In many GPR applications, near-field footprint plays a vital role since radar imaging can be improved when the size of the footprint is comparable to those of the targets. [5] Apart from the features mentioned above, there are many other requirements for a predominant GPR antenna. In short, low-frequency radiation, broad matching band, low profile, focused radiated field, low dispersion, and short ring-down are all to be satisfied.

Till now, many types of antennas for GPR applications are studied and designed. These antennas can be divided into two distinctive types by structural design. First are air-coupled antennas such as horn antennas [6], [7], the tapered slot antennas (TSA), and their variants [8], [9], which are normally 40-50 cm above the ground surface. Another type concludes many planar antennas that are suitable for working close to the ground, such as loaded dipole [10], spiral [11], [12], microstrip monopole [2], [13], [14], the bowtie antenna and its variants [15], [16]. The ground-coupled antennas could work tightly against or 5-10cm above the ground surface. As mentioned above, the frequency limitation is also a size limitation of the antenna. Horn antenna, such as TEM horn, has a length of half the longest wavelength. And its efficiency is decided by the area of the aperture. [7] For TSA, the dispersion in the frequency domain is unstable and the profile is also huge. [17] To obtain a stable phase center and low distortion, the spiral antenna is also excluded by impulse GPR. Then in the type of planar UWB antenna, microstrip monopole, planar dipole, and their variants are main representations. In the last few years, various designs of these planar antennas for GPR systems have been proposed. They have low cost and size as well as lightweight.

Bowtie antenna (BA), as a kind of planar dipole or biconical, has a more symmetric radiation pattern than planar monopole, though the pattern is omnidirectional if without a proper reflector. They have simple structures, linear-phase characteristics, and stable radiation. Various projects have been carried out by researchers all over around the world to develop BA applied for GPR.

The loading technique, as a useful method to improve BA, has been widely studied. Diego *et al.* employed layered absorbing material to achieve an ultra-wideband behavior. [3] Adrian *et al.* used fewer resistors to improve pulse radiation than the Wu-King loading profile. [18] Recently, simple resistance loading methods were still applied to design BA. [19] However, radiation efficiency, which is also vital for P-band GPR, will be lowered by lossy resistors. Adrian *et al*. also investigated the performance of capacitive loading and RC hybrid loading techniques. It was found that the hybrid loading maintains higher radiation efficiency and satisfactory late-time ringing at the same time. [20] Besides, a lumped resistor-inductance hybrid loading method was proposed. [21] But this scheme is unable to provide UWB performance, which makes it less suitable for GPR BA.

The radiation and matching characteristics are partly influenced by patch shape. Many BAs and bowtie slot antennas (BSAs) which had a triangular structure were designed because of the frequency-independent feature. [22], [23] But they suffered from reflections at the sharp antenna end. [24], [25] According to conformal analysis, the advanced BAs were usually modified to elliptical or half elliptical structures because they have less characteristic impedance and smooth paths for current to flow. [26]–[28] Folded Bowtie antenna (FBA) is a kind of loop loading antenna, which is similar to slot structure. The FBA is formed by connecting the two arms of a BA with two folding arms. And it can provide flatter input impedance and be easily matched in a wide frequency band. [29], [30] Traditionally, to form unidirectional radiation at boresight, a large metallic reflector is always needed for BA. The reflector is far bigger than the radiator, leading to a large profile of cavity-backed BA. [31]–[33] Recently Mohammed *et al.* proposed a bent FBA with compact back cavity. [34] However, the low cut-off frequency is still high even if the resistive loading method is utilized.

The aforementioned antennas commonly have an improving radiation efficiency as the frequency increases. And they have a lower cut-off frequency as the size increases. Thus, the requirements of high radiation efficiency and low-frequency radiation together lead to a large antenna size in terms of electrical length. Moreover, to separate the radiating part from the reflective cavity and ensure a minimal effect from the coupling, the patches of some antennas are elevated by the feeding structures. [29], [30] The structural stability will be reduced by this action. The galvanic connection of the antenna will be easily destroyed by the vibration generated during B-scan. Therefore, an investigative study by discussing a novel type of compact RC loaded FBA for P-band GPR is presented in this work. A 3-D loop circuit is formed by a double-layer loading scheme and ellipse-arc shape aiming to unprecedentedly expand the low cut-off frequency of FBA. Special tightly-coupled back-cavity is also designed to realize the miniaturization, matching at low band, unidirectional radiation, and sufficient mechanical support

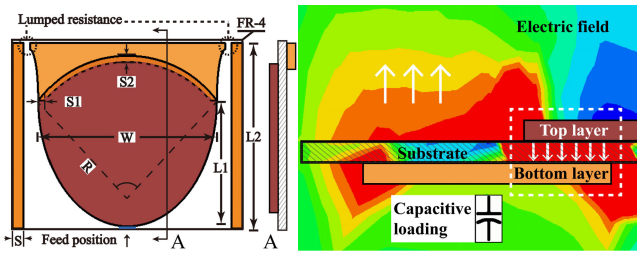

FIGURE 1. (a) Half piece of the proposed antenna patch. (Brown part: Top layer; Orange part: Bottom layer) (b) Topology of double-layer capacitive loading structure.

for the antenna. The final antenna covers a main operating band from 250 MHz to 850MHz with good matching at lower frequencies. Evaluation of its performance is done through numerical analysis and verified through measurements.

The present contribution is organized as follows. In Section II, the novel mechanism of hybrid loading, detailed design of the proposed antenna, and parametric study are elaborated. Section III presents the simulated performance and measured results of the fabricated prototype. The proposed antenna is compared with the triangular planar BA (TPBA) with similar geometry in section IV. In this section, a comparison of the proposed antenna with other designs is also provided to verify its superiority. Section V draws the conclusion.

II. ANTENNA DESIGN AND INNOVATION

A. CONCEPT AND TOPOLOGY

Promoting efficiency while maintaining bandwidth is a key challenge in antenna miniaturization. The operating bandwidth is limited by the impedance feature at first. As mentioned in section I, the proper design of patch shape is vital for keeping a stationary impedance curve in frequency domain. Because the input impedance of the BA is inversely proportional to the flare angle, the elliptical shape provides a small characteristic impedance and a smooth path for the current flow across the antenna. Hence, the elliptical structure or half elliptical structure is chosen as the shape of bowtie arm in the advanced design of BA used for the GPR applications. [35] In this paper, therefore, a combination of half ellipse and arc is utilized to form the patch on the top layer, as shown in Fig. 1(a). The copper is etched on a substrate made of 1 mm FR-4 with a relative dielectric constant of 4.4 and a loss tangent of 0.02. Another independent arc is used on the bottom layer to couple the current and expand the radiation surface. The copper on both sides would overlap in the vertical direction. An acorn shape with capacitive loading structure is then formed. The schematic of the capacitive loading is presented in Fig. 1(b). Current flows along the edge of the patch over the top layer and meets this circle gap. Subsequently, the current transfers to the bottom layer and is attenuated by the resistances. By applying this shape, reflection around the center of the patch end is minimized. Every single lumped resistance value is chosen to be 100 Ω.

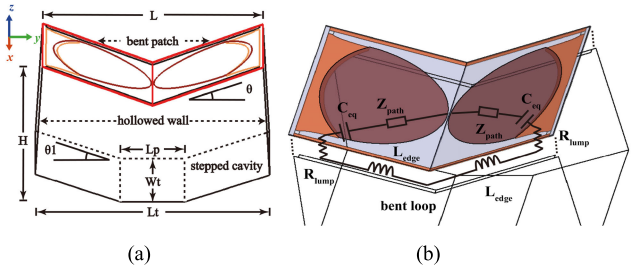

FIGURE 2. (a) Total geometry of the proposed antenna. (b) Topology of 3-D magnetic loop structure (bent FBA).

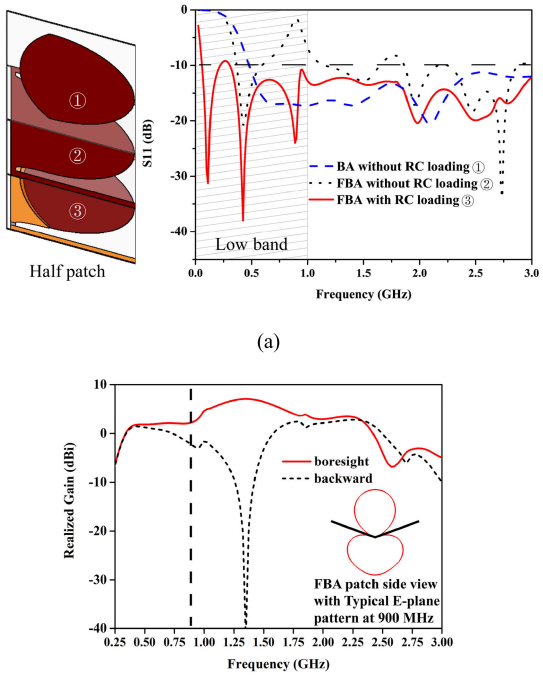

FIGURE 3. (a) The S-parameter (S_{11}) results of different BA patches. (b) Forward and backward gain of the bent FBA patch.

The antenna input impedance of around 100 Ω over an extremely wide band is realized by combining the same two half pieces to an FBA.

The bent FBA and the total antenna with a cavity are shown in Fig. 2(a). The folded bowtie patch is bent at an angle and placed on the cavity. As mentioned above, two same acorn-shaped pieces are connected at both sides on the bottom layer and angular placed. The 3-D magnetic loop is formed and shown in Fig. 2(b). Hybrid utilization of RC-loading is contained in the loop. The S-parameter (S_{11}) results of this novel FBA without reflector are shown in Fig. 3(a). For comparison, the performances of simple BA without RC loading, as well as FBA with and without RC loading, are simulated and shown. These patches have similar shapes as displayed on the left side of Fig. 3(a). The BA without RC loading shows a smooth curve and covers a wide band from 500 MHz to over 3 GHz. However, for P-band GPR application, this large profile has no advantage. The low

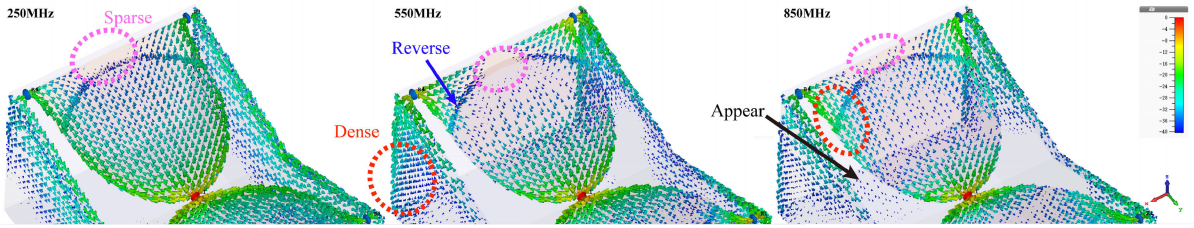

FIGURE 4. The surface current of AFBA at 250 MHz, 550 MHz, and 850 MHz.

cut-off frequency of FBA without RC loading is reduced to below 400 MHz, but two bandgaps are occurring at near 900 MHz and near 1800 MHz. This phenomenon stems from the electric current conflict between the patch shape and the FBA form. Thus, the single-layer structure is equivalent to four notches loaded at the center of the patch edge. By applying the proposed hybrid loading method to the simple FBA, we finally achieve a much lower cut-off frequency of 60 MHz. Matching at high frequency is also optimized. The final patch covers an ultra-wideband from 60 MHz to above 3 GHz. While extending the electrical length of the BA, the bent structure also focuses the boresight radiation. In Fig. 3(b), the realized gain of the novel bent FBA at boresight and backward is presented. With a bending angle of 20 degrees, the differences begin to be significant above 400 MHz and gradually enlarge with increasing frequency. The maximum front-to-back ratio (FBR) occurs at around 1.45 GHz. Then the differences become to be small. A typical E-plane pattern at 900 MHz is given under the gain curve. It is shown that the forward main lobe is focused and the back lobe is dispersed. In this paper, a part of bandwidth from 0.1 GHz to 1 GHz is interested and used for further design.

The complete antenna which is called Acorn FBA (AFBA) is realized by combining the FBA patch with a stepped side-absorbing structure. To maintain the bandwidth while weakening the backward radiation, cavities or reflectors with large profiles are applied by conventional BAs. In this paper, an H-plane narrowed cavity with stepped profile is proposed to further increase the total gain at high frequency. Different from the existed design, the E-plane sidewall of this novel cavity is hollowed, the H-plane side is electrically connected, and the bottom wall is stepped. The antenna has a strong near field in the hollowed area. To ensure that the reflection at low frequencies is minimized, the E-plane side is hollowed and the H-plane side is regarded as an extension of the current loop. By absorbing the side current of the magnetic loop, the reflection is further lowered and the H-plane pattern of the proposed AFBA is narrowed. At the same time, the cavity-backed AFBA is miniaturized without extending its width on the x-axis. Meanwhile, by using the stepped cavity instead of the flat cavity, a higher peak gain is achieved. The height of the back cavity is the result of comprehensive consideration of antenna size and maximum gain. The distance from the feed point to the back wall of cavity is chosen to be one-quarter of the wavelength at the center frequency. Thus, the total height of the proposed antenna is 180 mm. The geometry of the total antenna is shown in Fig. 2(a) and the surface currents at three key frequencies of 250 MHz, 550 MHz, and 850 MHz is shown in Fig. 4. The maintaining of the bandwidth is achieved by inserting the cavity to the patch. At all frequencies, the current on the bottom layer of the patch turns to be reverse for a moment and further propagates to the back of the cavity. The current distribution is changed by the additional phase lag caused by the RC-loading. Thus, the bandgaps occurring at 900 MHz and 1800 MHz mentioned above are solved by this hybrid loading method. In all situations, there is no reflection at the center of the patch end. This characteristic ensures the wide band to be extended towards low frequency. Besides, it is viewed that the higher the frequency is, the greater the range of current extending to the back cavity. At 250 MHz, the loop circuit is partly extended to the sidewall of the cavity. At 550 MHz, the current around the sidewall, especially around the hollowed edge of the cavity is dense. The excess current not absorbed by the resistor causes additional backward radiation. At 850 MHz, extra current is induced on the back wall of the cavity, which will cause the antenna's backward pattern to change again.

B. PARAMETRIC STUDY

To enhance the understanding of the antenna operating principle, a detailed parametric study has been carried out considering effects of vital structural parameters on the antenna performance. At first, the optimized parameters are given in Table 1. In this section, the numerical study is processed by Ansys HFSS.

As a common consideration, the radiation performance of the bent Acorn FBA patch is mainly influenced by the bending angle θ. As shown in Fig. 5(a) and Fig. 5(c), the effects of the bending angle to the S-parameter (S_{11}) and directivity of the FBA patch are analyzed. For $\theta = 0°$, the planar FBA radiates the same power in front and back. As θ increases, the reflection coefficient turns to be slightly worse, and the resonance characteristic moves to a higher frequency. Meanwhile, the boresight beam is focused, resulting in a higher directivity. For the case of $\theta = 30°$ in Fig.5(a), the S_{11} is worse than in other cases. In Fig. 5(b), it is seen that the cases of $\theta = 20°$ and $\theta = 30°$ have similar boresight directivity. After inserting the proposed back cavity to the FBA patch, the same scan of bending angle to the total antenna is done. The bending angle of the radiating patch is changed while the maximum height and the structure of the back panel are kept

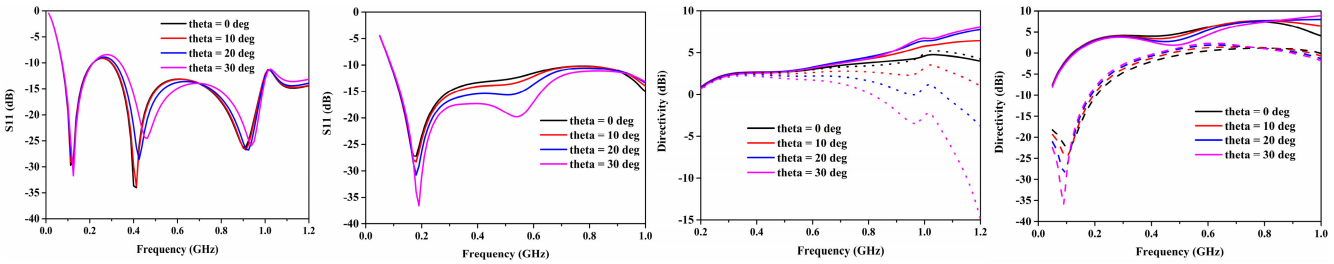

FIGURE 5. (a) S-parameter (S_{11}) of the proposed bent FBA patch at different θ. (b) S-parameter (S_{11}) of the total antenna at different θ. (c) The directivity of the bent FBA patch at different θ. (d) The directivity of the total antenna at different θ (solid lines are boresight directivities and dot/dash lines are backward directivities).

TABLE 1. Optimized design parameters for the proposed AFBA.

Antenna Element	Parameter	Value
Acorn FBA Patch	L1	98.4 mm
	L2	145.364 mm
	W	140 mm
	R	87.726 mm
	S	5 mm
	S1	5 mm
	S2	5 mm
Hollowed Stepped Side-absorbing Cavity	L	282 mm
	Lt	300 mm
	Lp	82.592 mm
	Wt	180 mm
	H	150 mm
	θ	20 deg
	θ1	20 deg

unchanged. The S11 result presented in Fig. 5(b) shows a different trend with Fig. 5(a). With the decreasing of the bending angle, the S11 continually getting worse. But from Fig. 5(d), the FBR at the central frequency increases. These differences come from the joint change of the radiation unit and the back-cavity structure. Considering that bending can bring better matching, high gain at high frequencies, and smaller near-field footprint, the solution of $\theta = 20°$ is finally chosen as a compromise between gain and antenna impedance matching. The effect of bending on the near-field footprint is put in Section III.

As the hollowed back cavity is inserted to the proposed FBA, another vital parameter S2 is analyzed to optimize the impedance matching. At the position of the novel arc capacitive-loading, the current is significantly influenced by the arc shape on the bottom layer. So S2 is the main factor that controlling the performance of capacitive-loading. As shown in Fig. 6, four profiles are corresponding to different values of S2, representing different situations of the novel capacitive-loading. The copper overlaps vertically on the top and bottom layer in profile 3 and 4 while changing to be tangent in

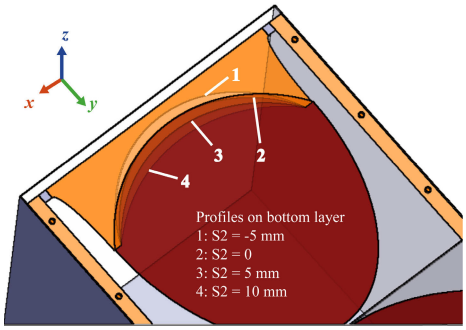

FIGURE 6. Different profiles effected by the parameter S2.

profile 2 and separate in profile 1. The structures of them are elaborated in the figure.

From Fig. 7(a), a significant changing trend of resistance and reactance with different values of S2 can be seen. The resistance at low frequencies increases with bigger values of S2, while the high-frequency situation is the opposite. There are two stagnation points on the real part curve at 450 MHz and 800 MHz. The reactance similarly has two stagnation points at 260 MHz and 620 MHz ignoring different values of S2. To ensure an impedance bandwidth covering the same frequency range as no back-cavity situation, the RC-loading parameters are chosen to maintain the flattest curve. So, the final value of S2 is decided to be 5 mm. Also, from the curves in Fig. 7(b), similar trend, and an added stagnation point can be seen both on the real and imaginary part curves with different values of the loaded resistor. Apart from significantly influencing the impedance matching of AFBA, applying different resistances of loading resistors will also change the radiation efficiency of AFBA. Considering all performances, the value of resistors is optimized to be 100 Ω, as mentioned in Section II-A.

III. ANTENNA COMPARISON AND MEASUREMENTS

At first, the common far-field characteristics of AFBA are shown in Fig. 8. The free space far-field 3-D patterns and the following near-field footprint results are calculated by CST microwave studio. The effectiveness of the stepped cavity is confirmed by the pattern at 250 MHz. Compared to the

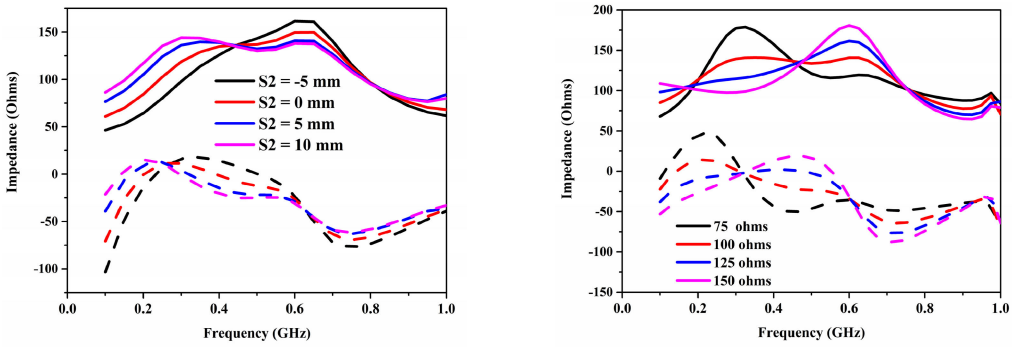

FIGURE 7. Influence of antenna parameters on the characteristic Impedance. (a) The overlap length S2. (b) The resistance of the loaded resistor. (solid lines are real parts and dash lines are imaginary parts).

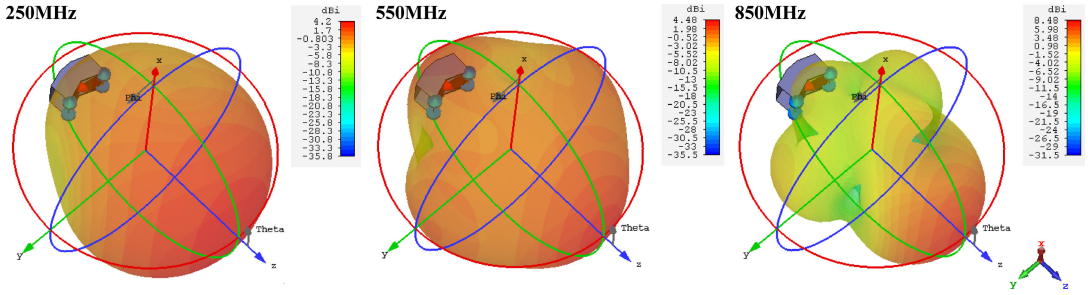

FIGURE 8. Far-field 3-D patterns in the free space at 250 MHz, 550 MHz and 850 MHz.

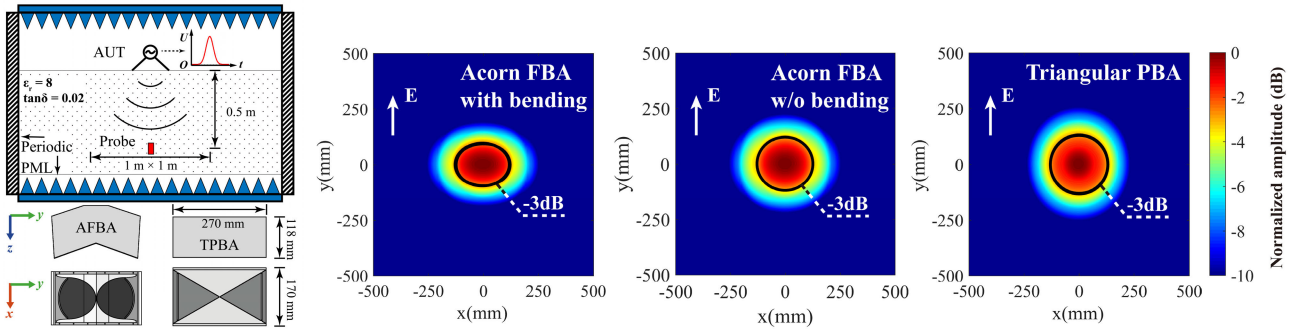

FIGURE 9. (a) Near-field footprint simulation scenario. (b) The near-field footprints of FBA and PBA.

FBR result of the proposed bent FBA patch in Fig. 3(b), forward directivity is improved while the backward radiation is reduced after inserting the novel back cavity. The radiating energy is slightly dispersed at 550 MHz because of the rising of the back lobe. As predicted in the explanations of Fig. 4, the current around the sidewall causes additional side lobe and back lobe. However, the main lobe still becomes narrower as the frequency goes up. At 850 MHz, the extra current induced on the back wall of the cavity disperses the energy of the back lobe. At the same time, the pattern is highly focused in the forward direction due to the increasing frequency. Compared to the results of no-cavity situation in Fig. 3(b) and Fig. 5(b), cavity-backed AFBA has more boresight radiation and less backward radiation.

In order to further demonstrate the superiority of the proposed antenna, a conventional TPBA with resistive-loading is simulated and fabricated as a comparison. In this paper, a helpful index to assess the radiating performance of GPR antennas called near-field footprint is used. An antenna footprint is defined as a distribution of the normalized peak values of transmit waveforms within a horizontal plane on the ground surface or subsurface, which indicates the shape and size of the spot illuminated by the antenna. [5] In this paper, a simulation scenario is built to inspect the near-field subsurface radiation of the two BAs, as shown in Fig. 9(a). In this schematic diagram, antennas under test (AUT) are fed with a signal of uni-polarity Guass pulse. The 10% pulse width is 2 ns. The AUT is faced with a simulated ground with

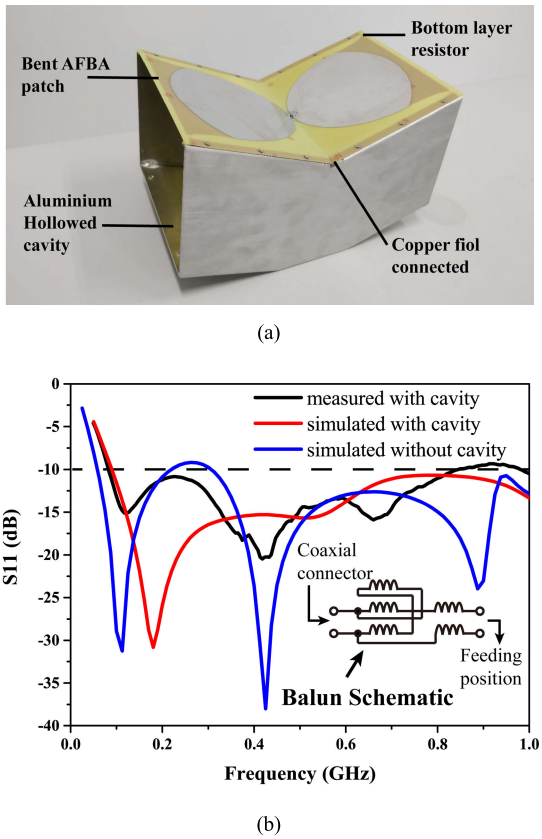

FIGURE 10. (a) The fabricated AFBA. (b) The S_{11} results of AFBA.

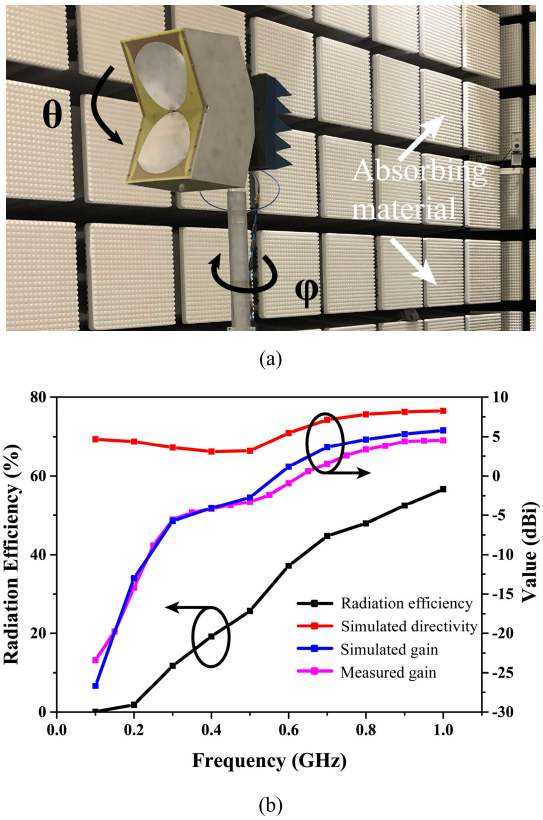

FIGURE 11. (a) The test scene in the microwave anechoic chamber. (b) Radiation efficiency, directivity, and gain of the bent FBA patch.

a loss tangent of 0.02 and a dielectric constant of 8. Periodic boundary and PML boundary are applied to simulate infinite ground and free space, respectively. At a distance of 0.5m under interface, a square with an area of 1 m×1 m is set to obtain E-field. In Fig. 9(b), the results with the direction of E-field is shown. The -3 dB footprints of the proposed AFBA with bending, the AFBA without bending, and TPBA are circled by black line. The pattern of AFBA with bending is similar to an ellipse with a semi-major axis of 120 mm and a semi-minor axis of 90 mm. The right two footprints are like perfect circles. But the result of AFBA without bending has a smaller radius of 120 mm, while the radius of TPBA result is 130 mm. The results above corroborate the narrowing of the far-field E-plane pattern and the effectiveness of bending the patch. Although bending also brings about a certain degree of deterioration in the FBR, it is beneficial for improving the resolution of GPR.

Based on the above results, the proposed AFBA and conventional TPBA were fabricated. As shown in Fig.10(a), copper is etched double-side on the FR-4 of which the thickness is 1mm. This kind of substrate has a loss tangent of 0.02 and a dielectric constant of 4.4. The bent patch is fixed to the aluminum back cavity with screws. At the feed position, a commercial wire balun produced by Mini-circuits is used to test the fabricated antenna. The 1:2 impedance ratio and desirable amplitude/phase balance are realized by this transmission-line transformer. The balun operates in a wide band of 30 MHz to 1800 MHz, covering the operating bandwidth of AFBA. In order to reveal its structure, the schematic provided by the datasheet is shown in Figure 10(b). It is made of enameled wires and a double-hole magnet core. The impedance of parallel lines is well designed to minimize the reflection caused by the impedance mismatch. Connecting the coaxial connector and the feeding point of the AFBA by this balun, the impedance is transformed from 50 Ω to 100 Ω. To measure the S_{11} of the proposed antenna, a vector network analyzer (VNA) named Keysight E5063A is used. The measured results are shown in Fig. 10(b). As mentioned above, the AFBA patch with hybrid RC-loading has UWB characteristics. After inserting the hollowed back cavity to the patch, the side of the loop is extended and the current is absorbed by the sidewall. Simulation results show that the proposed AFBA covers a wideband from 100 MHz to 1100 MHz. But in measurement, S_{11} above 850 MHz is slightly worse than simulation. Considering the signal used in the application, this result is still acceptable. The low cut-off frequency ensures less reflection when Gauss pulse is fed to the antenna.

The far-field characteristics of the proposed antenna are measured in the microwave anechoic chamber. The testing scenario is shown in Fig. 11(a). Two fabricated prototypes are used to obtain the measured results. From Fig. 11(b), the simulated radiation efficiency and directivity of the proposed antenna are shown. The simulated gain is calculated by

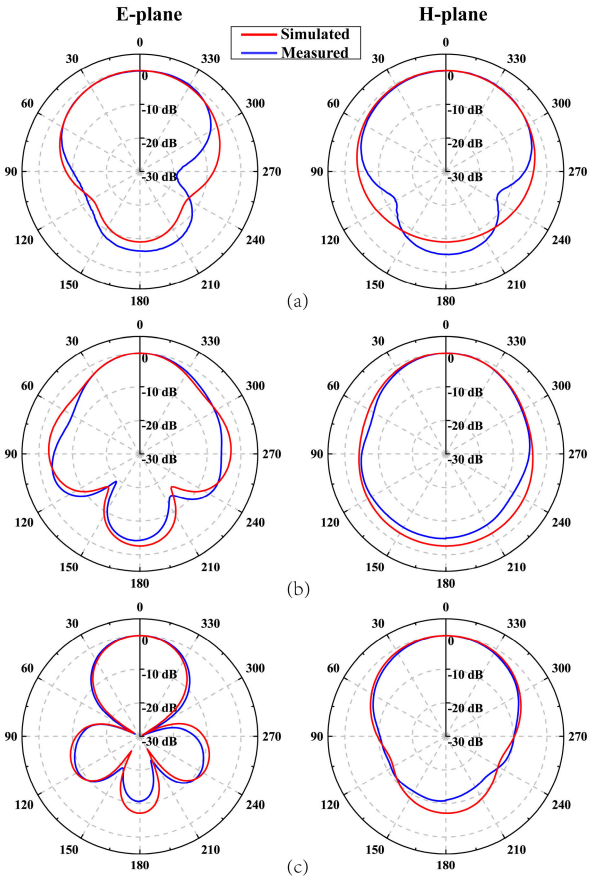

FIGURE 12. The normalized radiation patterns of E-plane and H-plane at (a) 250 MHz, (b) 550 MHz, and (c) 850 MHz.

multiplying the antenna efficiency and the antenna forward directivity. The measured forward gain is compared with the calculated gain result. The measured gain is equivalent to the simulated one below 500 MHz. As the frequency continues to rise, the loss caused by actual fabrication and insertion loss of balun increases, resulting in smaller measured results. At 850 MHz, the simulated gain achieves 5.2 dBi, while the measured one is only 4 dBi. After inserting the novel back cavity into the AFBA patch, the total efficiency is lowered because of the insufficient cavity height. However, it still higher than conventional loaded BA. The low cut-off frequency of 250 MHz is then defined where the efficiency is above 10% according to the result. The normalized radiation patterns both in E-plane and H-plane are shown in Fig. 12. The results contain simulated and measured patterns at three frequency points, which are 250 MHz, 550 MHz, and 850 MHz. At 250 MHz, the measured patterns of the fabricated antenna have a lower FBR compared to the simulated ones. However, the results obtained at the other two frequency points are opposite. Discrepancies between measurements and simulations are due to the physical differences between the computational models and fabricated prototypes and the range imperfections, including alignment error and tower bounce. Further tests are divided into two

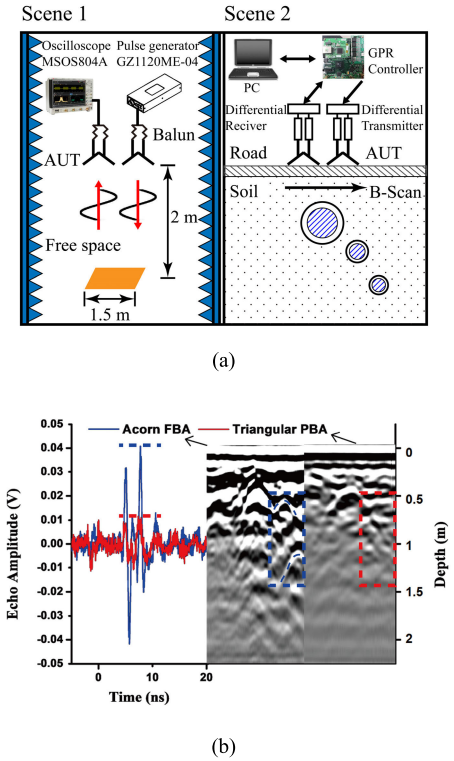

FIGURE 13. (a) The measurement scenarios of the antenna comparison. (b) The echo data from air and underground.

measurement scenarios. In the first scene on the left side of Fig. 13(a), the wideband balun mentioned before is still used. A piece of copper-clad laminate (CCL) in square shape is placed at 2 m away from the AUTs. The transmitting antenna is fed with an external pulse generator called GZ1120ME-04. A series of monocycle pulses with amplitude over ±25 V are generated and then attenuated by an attenuator. The central frequency of the spectrum is around 400 MHz. The echo from the CCL is received by receiving antenna and recorded by an oscilloscope named Keysight MSOS804A. The AUT is set to be AFBA and TPBA. The measured results are shown as the blue and red solid lines at the left of Fig. 13(b), respectively. In the same test scenario, the maximum echo received by AFBA is four times as that of resistive-loading TPBA. The free space result shows that the proposed antenna has a much higher radiation efficiency than conventional P-band BA.

On the right side of Fig. 13(a), a schematic depicts the scenario of integrated GPR and the road test. The wideband balun, pulse source, and oscilloscope are replaced with balanced transmitter and receiver. The amplitude of the uni-polarity Guass pulse generated by a transmitter can be increased to 40 V without applying attenuation. The control of the GPR prototypes is realized by an FPGA based controller. The controller communicates with PC via net wire, achieving the final processing and display of B-scan results. In the soil under road surface, a heating pipe and two sewer pipes are buried together. From the received B-scan data shown on the right side of Fig. 13(b), a clear underground

TABLE 2. Comparison between the proposed antenna and reported BAs with different mechanisms.

Ref.	Antenna structure	Size at the longest wavelength	Operating bandwidth	Peak efficiency/Gain
[20]	Circular-end RC-loaded BA	0.83λ × 0.67λ	150%	-/6 dBi
[24]	Triangular resistive-loaded BSA	0.55λ × 0.35λ	159%	-/5.4 dBi
[27]	Continuous resistive-loaded half-elliptical BA	0.28λ × 0.1λ× 0.018λ	100%	22%/-
[29]	Triangular reflector-backed FBA	0.95λ × 0.55λ × 0.18λ	58.6%	-/9.4 dBi
[34]	Triangular resistive-loaded bent FBA	0.78λ × 0.6λ × 0.37λ	100%	-/12 dBi
This work	Acorn shaped RC-loaded bent FBA	0.25λ × 0.15λ × 0.125λ	109.1%	50%/4 dBi

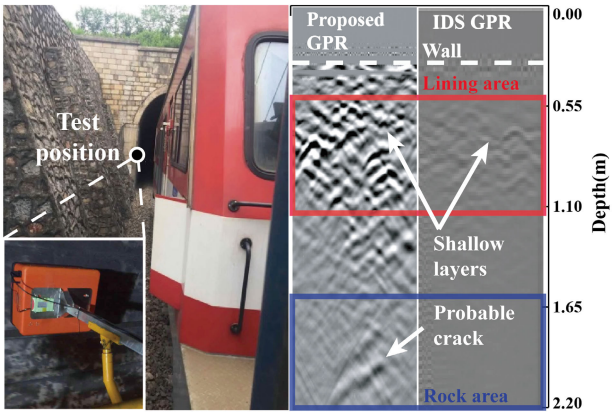

FIGURE 14. Tunnel lining test using the proposed AFBA-GPR and IDS GPR.

surrounding is depicted by proposed AFBA, including the layered structure and the buried pipes. Processed by the same methods, including band-pass filtering from 200MHz to 850MHz, DC removing and equal dynamic gain regulation enhancement, echo data obtained by TPBA shows a shallower detection distance, poorer resolution, and lower echo amplitude. Especially for the two thinner pipes, the deep burial depth and tiny distance to the main pipe make them difficult to be detected. As shown in Fig. 13(b), the two echoes marked in the blue dotted frame almost cannot be found in the red frame. The relatively high efficiency and narrow time-domain footprint are verified by the test results above.

After being tested on the road, the proposed GPR prototype and a commercial GPR produced by IDS GeoRadar with a central frequency of 400MHz are applied for another tunnel lining test. Based on the prior knowledge, the tunnel wall is made of two layers of normal concrete. There will be uneven layering inside the wall because of aging. If there exist some void holes or the contact between the two layers is not dense, it is easy to cause an accident in the tunnel. Using GPRs to detect the wall in tunnel can help to find these problems. In Fig. 14, an experiment scene of a tunnel lining test is presented on the left side. The proposed AFBA-GPR is firmly fixed to one side of the train and detects the lining of the entire tunnel as the train moves at a constant speed. The same process is done with commercial GPR. On the right side of Fig. 14, the processed data obtained by two GPRs together display the uneven multiple reflection characteristics which are caused by the loose contact or discontinuity. After applying the same signal processing flow, the B-scan image obtained by the proposed GPR has a clearer reflected echo. Meanwhile, the proposed radar even gets echoes that might be cracks in the deeper rock layer, which further corroborates the enhanced radiation of the proposed AFBA. This result also proves the practicability of the antenna in the GPR applications.

IV. DISCUSSION

The proposed AFBA is designed for improving the radiation performance of P-band GPR antenna. As mentioned in Section I, there are many kinds of conventional BAs designed in different considerations, and according to different mechanisms. The proposal of a multilayer RC-loading structure used for FBA is a try to improve the low-frequency bandwidth and radiation efficiency of BA. For P-band GPR, the size of the antenna and the detection depth remain the most important issues. To further discuss the feature of the novel structure, Table 2 presents a comparison between the proposed antenna and different BA designs reported in the open literature. For non-loaded BAs such as [29], the efficiency is extremely high but miniaturization is hard to realize. Meanwhile, the bandwidth is not wide enough for GPR applications. For conventional resistive-loaded BAs such as [27], the promotion of antenna efficiency is hard work. But for the BAs using RC-loading method such as [20], the large profile of the antenna limits the application. In recent years, BSAs such as [24] began to be used in GPR. But the low cut-off frequency of these antennas is still high and hard to be lowered. [25] In the last year, a triangular resistive-loaded bent FBA is proposed, it is possible to improve the detection depth by the high gain. However, the soil underground is a lossy medium, so reducing the operating frequency is also meaningful. By introducing a novel loading method to FBA, the proposed AFBA patch realizes a flat impedance curve from 60 MHz to 3 GHz, which is wider than the results from state-of-art FBAs. By applying a novel back cavity, the proposed AFBA maintains a considerable bandwidth without using absorber. The measured relative bandwidth is defined as 109.1% from 250 MHz to 850 MHz, according to the

S11 results and efficiency at low frequency. The peak efficiency of 50% is simulated radiation efficiency ignoring the loss of balun structure. The peak gain of 4 dBi is obtained by the measurement mentioned in Fig. 11. Meanwhile, the maximum electrical length of the AFBA is smallest in Table 2. The performance of the integrated GPR is tested in the real application.

V. CONCLUSION

In this paper, an acorn-shaped bent folded bowtie antenna with a back cavity has been proposed. A novel arc-shaped distributed multilayer capacitive loading structure is combined with resistive loading. The front beam of the patch is focused and the bandwidth is significantly increased to 60 MHz-3 GHz. A novel technique of cavity groove is proposed to design the reflector. Without applying any absorber, the bandwidth is maintained and the pattern is further shaped after inserting a novel cavity. The radiation mechanism and the surface current are discussed. The optimization of the bending angle and the loading structure are revealed. Far-field patterns and near-field footprint are considered at the same time. The operating bandwidth is defined from 0.25 GHz to 0.85 GHz, covering most of the P-band. The characteristics of the proposed antenna are verified both by numerical and measurement results. Furthermore, field tests for practical ground-penetrating radar (GPR) applications have been carried out and the results demonstrate the advanced performance.

REFERENCES

[1] D. Daniels, *Ground Penetrating Radar*, 2nd ed. Piscataway, NJ, USA: IEEE Press, 2004.

[2] A. Raza, W. Lin, Y. Liu, A. B. Sharif, Y. Chen, and C. Ma, "A magnetic-loop based monopole antenna for GPR applications," *Microw. Opt. Technol. Lett.*, vol. 61, no. 4, pp. 1052–1057, Apr. 2019.

[3] D. Caratelli, A. Yarovoy, and L. P. Ligthart, "Full-wave analysis of cavity-backed resistively loaded bow-tie antennas for GPR applications," in *Proc. Eur. Radar Conf.*, Amsterdam, The Netherlands, Oct. 2008, pp. 204–207.

[4] C. A. Balanis, *Antenna Theory: Analysis and Design*, 4th ed. New York, NY, USA: Wiley, 2016.

[5] A. A. Pramudita, A. Kurniawan, A. B. Suksmono, and A. A. Lestari, "Effect of antenna dimensions on the antenna footprint in ground penetrating radar applications," *IET Microw., Antennas Propag.*, vol. 3, no. 8, pp. 1271–1278, Dec. 2009.

[6] M. A. Salari, O. Manoochehri, A. Darvazehban, and D. Erricolo, "An active 20-MHz to 2.5-GHz UWB receiver antenna system using a TEM horn," *IEEE Antennas Wireless Propag. Lett.*, vol. 16, pp. 2432–2435, Jan. 2017.

[7] A. A. H. Ameri, G. Kompa, and A. Bangert, "Study about TEM horn size reduction for ultrawideband radar application," in *Proc. German Microw. Conf.*, Darmstadt, Germony, Mar. 2011, pp. 1–4.

[8] Y. Liu, W. Zhou, S. Yang, W. Li, P. Li, and S. Yang, "A novel miniaturized vivaldi antenna using tapered slot edge with resonant cavity structure for ultrawideband applications," *IEEE Antennas Wireless Propag. Lett.*, vol. 15, pp. 1881–1884, Mar. 2016.

[9] J. Liu, J. Geng, K. Wang, Z. Ding, J. Li X. Zhao, R. Jin, X. Liang, and W. Zhu, "A low-profile, directional, ultrawideband antenna," *IEEE Antennas Wireless Propag. Lett.*, vol. 18, no. 2, pp. 255–259, Feb. 2019.

[10] M. Bod, M. Ahmadi-Boroujeni, and K. Mohammadpour-Aghdam, "Design of a low-cost broadband loaded dipole antenna for VHF/UHF frequency range," *IET Microw., Antennas Propag.*, vol. 13, no. 12, pp. 1983–1988, Oct. 2019.

[11] B. A. Kramer, C.-C. Chen, and J. L. Volakis, "Size reduction of a low-profile spiral antenna using inductive and dielectric loading," *IEEE Antennas Wireless Propag. Lett.*, vol. 7, pp. 22–25, Feb. 2008.

[12] T.-Y. Shih and N. Behdad, "A compact, broadband spiral antenna with unidirectional circularly polarized radiation patterns," *IEEE Trans. Antennas Propag.*, vol. 63, no. 6, pp. 2776–2781, Jun. 2015.

[13] S. Kundu and S. K. Jana, "A compact umbrella shaped UWB antenna for ground-coupling GPR applications," *Microw. Opt. Technol. Lett.*, vol. 60, no. 1, pp. 146–151, Jan. 2018.

[14] A. Raza, W. Lin, Y. Chen, Z. Yanting, H. T. Chattha, and A. B. Sharif, "Wideband tapered slot antenna for applications in ground penetrating radar," *Microw. Opt. Technol. Lett.*, vol. 62, no. 7, pp. 2562–2568, Jul. 2020.

[15] S.-G. Zhou, G.-L. Huang, and T.-H. Chio, "A low profile, wideband cavity-backed bowtie antenna," *Microw. Opt. Technol. Lett.*, vol. 55, no. 6, pp. 1422–1426, Jun. 2013.

[16] S.-W. Qu, C.-H. Chan, and Q. Xue, "Ultrawideband composite cavity-backed folded sectorial bowtie antenna with stable pattern and high gain," *IEEE Trans. Antennas Propag.*, vol. 57, no. 8, pp. 2478–2483, Aug. 2009.

[17] M. Moosazadeh, S. Kharkovsky, J. T. Case, and B. Samali, "Miniaturized UWB antipodal Vivaldi antenna and its application for detection of void inside concrete specimens," *IEEE Antennas Wireless Propag. Lett.*, vol. 16, pp. 1317–1320, 2017.

[18] A. A. Lestari, E. Bharata, A. B. Suksmono, A. Kurniawan, A. G. Yarovoy, and L. P. Ligthart, "A modified bow-tie antenna for improved pulse radiation," *IEEE Trans. Antennas Propag.*, vol. 58, no. 7, pp. 2184–2192, Jul. 2010.

[19] Y. Wu, F. Shen, Y. Yuan, and D. Xu, "An improved modified universal ultra-wideband antenna designed for step frequency continuous wave ground penetrating radar system," *Sensors*, vol. 19, no. 5, p. 1045, Mar. 2019.

[20] A. A. Lestari, A. G. Yarovoy, and L. P. Ligthart, "RC-loaded bow-tie antenna for improved pulse radiation," *IEEE Trans. Antennas Propag.*, vol. 52, no. 10, pp. 2555–2563, Oct. 2004.

[21] A. Zou, J. Li, K. Wang, and D. Cheng, "Investigations of RL-loaded bowtie antenna for low-resolution GPR," in *Proc. 5th Int. Conf. Wireless Commun., Netw. Mobile Comput.*, Beijing, China, Sep. 2009, pp. 1–3.

[22] X. Li, M. Jalilvand, Y. L. Sit, and T. Zwick, "A compact double-layer on-body matched bowtie antenna for medical diagnosis," *IEEE Trans. Antennas Propag.*, vol. 62, no. 4, pp. 1808–1816, Apr. 2014.

[23] S.-E. Hamran, T. Berger, S. Brovoll, L. Damsgard, O. Helleren, M. J. Oyan, H. E. Amundsen, L. Carter, R. Ghent, J. Kohler, M. Mellon, D. Paige, D. Plettemeier, and J. Eide, "RIMFAX: A GPR for the mars 2020 rover mission," in *Proc. 8th Int. Workshop Adv. Ground Penetrating Radar (IWAGPR)*, Florence, Italy, Jul. 2015, pp. 1–4.

[24] F. Sagnard, "Design of a compact ultra-wide band bow-tie slot antenna system for the evaluation of structural changes in civil engineering works," *Prog. Electromagn. Res. B*, vol. 58, pp. 181–191, Feb. 2014.

[25] V. S. Bhaskar, E. L. Tan, and L. K. H. Holden, "Design of wideband bowtie slot antenna using sectorially modified gielis curves," *IEEE Antennas Wireless Propag. Lett.*, vol. 17, no. 12, pp. 2237–2240, Dec. 2018.

[26] B. Wu, Y. Ji, and G. Fang, "Analysis of GPR UWB half-ellipse antennas with different heights of backed cavity above ground," *IEEE Antennas Wireless Propag. Lett.*, vol. 9, pp. 130–133, 2010.

[27] X. Li, Y. Ji, W. Lu, and G. Fang, "Analysis of GPR antenna system mounted on a vehicle," *IEEE Antennas Wireless Propag. Lett.*, vol. 12, pp. 575–578, 2013.

[28] J. Shao, G. Fang, Y. Ji, and H. Yin, "Semicircular slot-tuned planar half-ellipse antenna with a shallow vee-cavity in vital sign detection," *IEEE J. Sel. Topics Appl. Earth Observ. Remote Sens.*, vol. 7, no. 3, pp. 767–774, Mar. 2014.

[29] Z.-Y. Zhang, S.-L. Zuo, and J.-Y. Zhao, "Wideband folded bowtie antenna with γ-shaped strip feed and tuning stubs," *Microw. Opt. Technol. Lett.*, vol. 55, no. 9, pp. 2145–2149, Sep. 2013.

[30] S.-W. Qu, J.-L. Li, Q. Xue, C. H. Chan, and S. Li, "Wideband and unidirectional cavity-backed folded triangular bowtie antenna," *IEEE Trans. Antennas Propag.*, vol. 57, no. 4, pp. 1259–1263, Apr. 2009.

[31] H. Wong, K.-M. Mak, and K.-M. Luk, "Wideband shorted bowtie patch antenna with electric dipole," *IEEE Trans. Antennas Propag.*, vol. 56, no. 7, pp. 2098–2101, Jul. 2008.

[32] Y. Wang, F. Zhang, X. Zhang, G. Fang, and Y. Ji, "RC-loaded planar half-ellipse antenna for impulse radar application," *Electron. Lett.*, vol. 51, no. 23, pp. 1841–1842, Nov. 2015.

[33] M. Joula, V. Rafiei, and S. Karamzadeh, "High gain UWB bow-tie antenna design for ground penetrating radar application," *Microw. Opt. Technol. Lett.*, vol. 60, no. 10, pp. 2425–2429, Sep. 2018.
[34] M. Serhir and D. Lesselier, "Wideband reflector-backed folded bowtie antenna for ground penetrating radar," *IEEE Trans. Antennas Propag.*, vol. 66, no. 3, pp. 1056–1063, Mar. 2018.
[35] R. Nayak and S. Maiti, "A review of bow-tie antennas for GPR applications," *IETE Tech. Rev.*, pp. 1–16, Jul. 2018.

GUANGYAO YANG (Student Member, IEEE) received the B.S. degree from Xidian University, Xi'an, China, in 2016. He is currently pursuing the Ph.D. degree with the School of Electrical and Electronic Engineering, University of the Chinese Academy of Sciences, Beijing, China.

His research interests include ultrawideband antennas, metamaterial, and MIMO radar design.

SHENGBO YE received the Ph.D. degree from the Institute of Electronics, Chinese Academy of Sciences (CAS), Beijing, China, in 2011. Since 2011, he has been with the Key Laboratory of Electromagnetic Radiation and Sensing Technology, CAS. His research interests include UWB through-wall radar detection, imaging, ground penetrating, radar signal processing, life detection, and other related applications.

YICAI JI received the B.S. and Ph.D. degrees from Xidian University, Xi'an, China, in 1998 and 2004, respectively.

From 2004 to 2006, he was a Postdoctoral Research Associate with the Xi'an University of Electronic Science and Technology. Since 2006, he has been an Associate Professor with the Key Laboratory of Electromagnetic Radiation and Sensing Technique, Chinese Academy of Sciences, Beijing, China. His research interests include ultrawideband antennas, computational electromagnetics, and ultrawideband radar.

XIAOJUAN ZHANG received the Ph.D. degree from the Institute of Electronics, Chinese Academy of Sciences (CAS), Beijing, China, in 2000.

Since 2000, she has been a Professor with the Institute of Electronics, CAS. From 2001 to 2002, she was a Postdoctoral Researcher with the University of Illinois at Urbana-Champaign, Champaign, IL, USA. She undertakes the National Natural Science Foundation of China, Beijing, major national scientific and technological projects in 863 key projects, CAS projects on important directions. She has authored or coauthored over 100 publications. Her research interests include electromagnetic wave scattering in inhomogeneous medium, inverse problem, microwave imaging and application, antenna technology, SAR systems, geophysics and electromagnetic detection methods, and computational electromagnetic.

GUANGYOU FANG received the B.S. degree in electrical engineering from Hunan University, Changsha, China, in 1984, and the M.S. and Ph.D. degrees in electrical engineering from Xi'an Jiaotong University, Xi'an, China, in 1990 and 1996, respectively.

From 1990 to 1999, he was an Engineer, an Associate Professor, and a Professor with the China Research Institute of Radiowave Propagation, Xinxiang, China. From 2000 to 2001, he was a Visiting Scholar with the University of Trieste, Trieste, Italy, and the International Center for Science and High Technology, United Nations Industrial Development Organization, Trieste. From 2001 to 2003, he was a Special Foreign Research Fellow of the Japan Society for the Promotion of Science, working with Prof. M. Satoat, Tohoku University, Sendai, Japan. Since 2004, he has been a Professor with the Institute of Electronics, CAS, Beijing, China, where he was the Director of the Key Laboratory of Electromagnetic Radiation and Sensing Technology and involved in the design of lunar penetrating radar for China's second lunar exploration project which has successfully obtained the field detection data, in 2013. He is currently leading a group to achieve the lunar structure detecting radar design for China's third lunar exploration project. He has authored over 100 publications. His research interests include ultra-wideband radars, ground-penetrating radar signal processing and identification methods, terahertz imaging technologies, and computational electromagnetics.